Dynamic Reconfiguration Manipulability Analyses of Redundant Robot and Humanoid Walking

Yosuke Kobayashi, Mamoru Minami, Akira Yanou and Tomohide Maeba

***Abstract*— In this paper, we propose a new index of dynamic manipulability for humanoid robot to estimate dynamic ability to change configuration by using remaining redundancy, while prior task is being controlled, e.g., face and eyes being directed to some object. Several indexes have been proposed so far to measure statical and dynamical capability of robot manipulator. For example, Dynamic Manipulability (DM) ellipsoid describes a distribution of hand acceleration produced by normalized joint torque. On the other hand, Reconfiguration Manipulability (RM) ellipsoid denotes a distribution of each link velocity produced by joint angular velocity. This paper shows new index of Dynamic Reconfiguration Manipulability (DRM) combined DM and RM, and we have adopted the DRM to a humanoid robot, exhibiting how the DRM indicates directly the configuration-changeability of walking humanoid robot.**

I. Introduction

As for walking control of the humanoid, ZMP-based walking is known as the most promising approach, which has been proved to be a realistic control strategy to demonstrate stable walking of actual biped robots, since it can guarantee that the robots can keep standing by retaining the ZMP within the convex hull of supporting area [1], [2]. Instead of the ZMP, another approaches that put importance on keeping the robot's walking trajectories inside a basin of attraction [3]-[5] including a method referring limit cycle to determine input torque [6].

These previous discussions are based on simplified bipedal models, which tend to avoid discussing the effects of feet or slipping existing in real world. Contrarily to the above references, a research [7] has pointed out that the effect of foot bears varieties of the walking gait, which dimension of the equation of motion varies according to contacting conditions to floor of feet standing or in the air. Our research has begun from such view point of [7] as aiming at describing dynamics of gait as correctly as possible, including surface or point-contacting state of foot and toe, slipping of the foot and heel-striking, where walking gait states based on the results of walking motions, called event-driven. And that what the authors think important is that the dimension of dynamical equation will change depending on motions of the walking gait (event-driven results), which has been discussed by [8] on one-legged hopping robot. Given as an example that heel be detached from ground while its toe being contacting, a new state variable describing rotation of foot would emerge, resulting in an increase of a number of state variables. In

Y. Kobayashi, M. Minami, A. Yanou and T. Maeba are with Graduate School of Natural Science and Technology, Okayama University, Okayama, Japan 700-8530 {kobayashi2, minami, yanou, maeba}@suri.sys.okayama-u.ac.jp

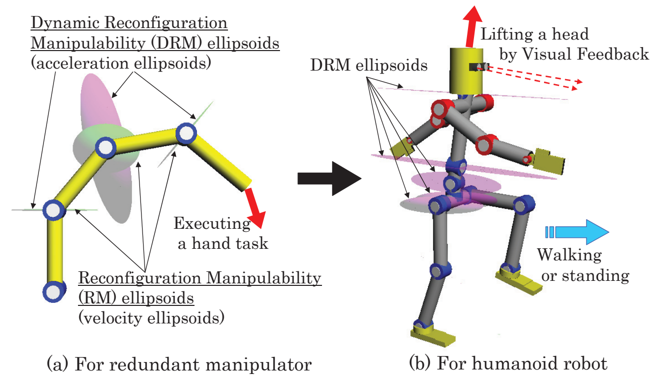

Fig. 1. Applications of dynamic reconfiguration manipulability

fact, this kind of dynamics with the dimension number of state variables being changed by the result of its dynamical transitions in time are out of the arena of control theory that discusses how to control a system with fixed number of states. Additionally, toe-off motion has been called as non-holonomic dynamics that includes a joint without inputting torque, i.e., free joint. Meanwhile, landing of heel or toe of lifting leg in the air to ground means a geometrical contact. Nakamura [9] mentioned how to represent contacting with environment that can handle constraint motion with friction by algebraic equation and applied it to human figures. We have derived dynamics of eleven kinds of gaits based on above references, especially along with [9].

To achieve a stable walking of humanoid robot without applying ZMP-based strategies, we have proposed "Visual Lifting Approach" strategy [12] and have confirmed that it can confine unstable toe-off state in a stable limit cycle, making the closed-loop walking dynamics stable. Humans can change whole configuration-height or horizontal trajectory of waist avoid obstacles while walking and gazing at something existing ahead. The humans' behavior utilizes redundancy as a result of primary task of walking and gazing. Therefore we want to discuss about dynamical redundancy of humanoid robot in this paper, proposing a dynamical reconfiguration manipulability (DRM) concept, which is a measure of how much a dynamical system can potentially produce a motion in a work space with normalized input torque, by combining the dynamic manipulability (DM) [14] with reconfiguration manipulability (RM) [15]. This new measure represents how much the dynamical system of robots possess shape-reconfiguration acceleration ability in workspace by unit torque input for all joints while executing primary tasks. The DRM have been applied to a humanoid robot, whose prior task be allocated to sustain head position to be high as much as possible. The concept is shown in

Fig. 1(b) and the DRM of floor-fixed four link robot is shown in Fig. 1(a). Simulations show the DRM varies with the human's waist position, suggesting that strategies can be applicable such as the whole configuration of robots' walking can be modified through DRM based on walking conditions as obstacles ahead.

II. Dynamic Reconfiguration Manipulability

A. Dynamic Manipulability

In general, equation of motion for serial link manipulators is written as

$$\boldsymbol{M}(\boldsymbol{q})\ddot{\boldsymbol{q}} + \boldsymbol{h}(\boldsymbol{q},\dot{\boldsymbol{q}}) + \boldsymbol{g}(\boldsymbol{q}) + \boldsymbol{D}\dot{\boldsymbol{q}} = \boldsymbol{\tau} \tag{1}$$

where $\boldsymbol{M}(\boldsymbol{q}) \in \mathrm{R}^{n\times n}$ is inertia matrix, $\boldsymbol{h}(\boldsymbol{q},\dot{\boldsymbol{q}}) \in \mathrm{R}^{n}$ and $\boldsymbol{g}(\boldsymbol{q}) \in \mathrm{R}^{n}$ are vectors which indicate Coriolis force, centrifugal force and gravity, $\boldsymbol{D} = diag[d_1, d_2, \cdots, d_n]$ is matrix which means coefficients of joints' viscous friction and $\boldsymbol{\tau} \in \mathrm{R}^{n}$ is joint torque. The kinematic equation of a robot, the relation of the i-th link's velocity $\dot{\boldsymbol{r}}_i \in \mathrm{R}^{m}$ to the angular velocity $\dot{\boldsymbol{q}} \in \mathrm{R}^{n}$ is represented by

$$\dot{\boldsymbol{r}}_i = \boldsymbol{J}_i\dot{\boldsymbol{q}} \quad (i = 1, 2, \cdots, n) \tag{2}$$

Then, $\boldsymbol{J}_i \in R^{m\times n}$ can be described as Jacobian matrix with zero block matrix, $\boldsymbol{J}_i = [\tilde{\boldsymbol{J}}_i,\ \boldsymbol{0}]$. By differentiating Eq. (2), we can obtain the following equation.

$$\ddot{\boldsymbol{r}}_i = \boldsymbol{J}_i(\boldsymbol{q})\ddot{\boldsymbol{q}} + \dot{\boldsymbol{J}}_i(\boldsymbol{q})\dot{\boldsymbol{q}} \tag{3}$$

where we can understand that $\dot{\boldsymbol{J}}_i(\boldsymbol{q})\dot{\boldsymbol{q}}$ is the acceleration as Coliolis and centrifugal acceleration resulted from nonlinear relation of two-coordinates-space represented by $\boldsymbol{q}_i$ to $\boldsymbol{r}_i$. Then, from Eqs. (1) and (3) we can obtain the following equation.

$$\ddot{\boldsymbol{r}}_i - \dot{\boldsymbol{J}}_i(\boldsymbol{q})\dot{\boldsymbol{q}} = \boldsymbol{J}_i\boldsymbol{M}^{-1}[\boldsymbol{\tau} - \boldsymbol{h}(\boldsymbol{q},\dot{\boldsymbol{q}}) - \boldsymbol{g}(\boldsymbol{q}) - \boldsymbol{D}\dot{\boldsymbol{q}}] \tag{4}$$

Here, two variables are defined as follows:

$$\tilde{\boldsymbol{\tau}} \triangleq \boldsymbol{\tau} - \boldsymbol{h}(\boldsymbol{q},\dot{\boldsymbol{q}}) - \boldsymbol{g}(\boldsymbol{q}) - \boldsymbol{D}\dot{\boldsymbol{q}} \tag{5}$$

$$\ddot{\tilde{\boldsymbol{r}}}_i \triangleq \ddot{\boldsymbol{r}}_i - \dot{\boldsymbol{J}}_i(\boldsymbol{q})\dot{\boldsymbol{q}} = \boldsymbol{J}_i(\boldsymbol{q})\ddot{\boldsymbol{q}} \tag{6}$$

Then, Eq. (4) can be rewritten as

$$\ddot{\tilde{\boldsymbol{r}}}_i = \boldsymbol{J}_i\boldsymbol{M}^{-1}\tilde{\boldsymbol{\tau}} \quad (i = 1, 2, \cdots, n) \tag{7}$$

Considering desired accelerations $\ddot{\tilde{\boldsymbol{r}}}_{id}$ of all links yielded by a set of joint torques $\tilde{\boldsymbol{\tau}}$ that satisfies an Euclidean norm condition, that is, $\|\tilde{\boldsymbol{\tau}}\| = (\tilde{\tau}_1^2 + \tilde{\tau}_2^2 + \cdots + \tilde{\tau}_n^2)^{1/2} \leq 1$, then the each tip acceleration shapes an ellipsoid in range space of $\boldsymbol{J}_i$. These ellipsoids of each link have been known as "Dynamic Manipulability Ellipsoid (DME)" [14] (Fig.2(a)) which are described as

$$\ddot{\tilde{\boldsymbol{r}}}_{id}^{T}[\boldsymbol{J}_i(\boldsymbol{M}^T\boldsymbol{M})^{-1}\boldsymbol{J}_i^T]^{+}\ddot{\tilde{\boldsymbol{r}}}_{id} \leq 1, \ \ and \ \ \ddot{\tilde{\boldsymbol{r}}}_{id} \in \mathrm{R}(\boldsymbol{J}_i) \tag{8}$$

where, $\mathrm{R}(\boldsymbol{J}_i)$ represents range space of $\boldsymbol{J}_i$.

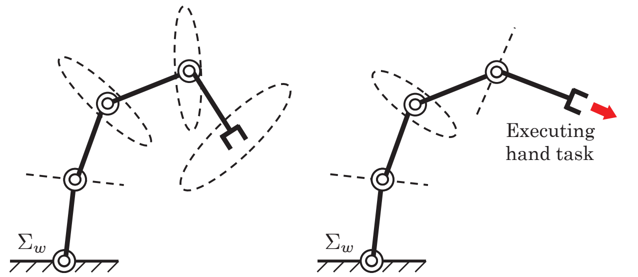

(a) Dynamic manipulability (DM) ellipses and segment
(b) Dynamic reconfiguration manipulability (DRM) ellipses and segments

Fig. 2. Dynamic manipulability and dynamic reconfiguration manipulability

B. Dynamic Reconfiguration Manipulability

Here we assume that the desired end-effector's acceleration $\ddot{\boldsymbol{r}}_{nd}$ are given as primary task. Relation between $\ddot{\tilde{\boldsymbol{r}}}_n$ and $\tilde{\boldsymbol{\tau}}$ is denoted to give $i = n$ into Eq. (7), then,

$$\ddot{\tilde{\boldsymbol{r}}}_n = \boldsymbol{J}_n\boldsymbol{M}^{-1}\tilde{\boldsymbol{\tau}} \tag{9}$$

Solving Eq. (9) for $\tilde{\boldsymbol{\tau}}$ yielding desired acceleration $\ddot{\tilde{\boldsymbol{r}}}_{nd}$

$$\begin{aligned}\tilde{\boldsymbol{\tau}} = {} & (\boldsymbol{J}_n\boldsymbol{M}^{-1})^{+}\ddot{\tilde{\boldsymbol{r}}}_{nd} \\ & + [\boldsymbol{I}_n - (\boldsymbol{J}_n\boldsymbol{M}^{-1})^{+}(\boldsymbol{J}_n\boldsymbol{M}^{-1})]\,{}^{1}\boldsymbol{l}\end{aligned} \tag{10}$$

${}^{1}\boldsymbol{l}$ is an arbitrary vector satisfying ${}^{1}\boldsymbol{l} \in \mathrm{R}^{n}$. The left superscript "1" of ${}^{1}\boldsymbol{l}$ means the first dynamic reconfiguration task. In the right side of Eq. (10), the first term denotes the solution making $\tilde{\boldsymbol{\tau}}$ minimize in the null space of $\boldsymbol{J}_n\boldsymbol{M}^{-1}$ during implementing $\ddot{\tilde{\boldsymbol{r}}}_{nd}$. The second term denotes the components of torques at each joint, which can change the shape of manipulator regardless with the influence of $\ddot{\tilde{\boldsymbol{r}}}_{nd}$ given arbitrarily as end-effector acceleration for tracking the desired trajectory.

Providing the first dynamic reconfiguration task, that is the first reconfiguration task ${}^{1}\ddot{\tilde{\boldsymbol{r}}}_{jd}$ $(j = 1, 2, \cdots, n-1)$, is given to the j-th link, shall we discuss realizability of ${}^{1}\ddot{\boldsymbol{r}}_{jd}$ in the following argument. In this research, ${}^{1}\ddot{\boldsymbol{r}}_{jd}$ is assumed to be commanded by an dynamic reconfiguration control system of higher level. We can obtain the relation of ${}^{1}\ddot{\tilde{\boldsymbol{r}}}_j$ and $\ddot{\tilde{\boldsymbol{r}}}_{nd}$ from Eqs. (7) and (10).

$$\begin{aligned}{}^{1}\ddot{\tilde{\boldsymbol{r}}}_j = {} & \boldsymbol{J}_j\boldsymbol{M}^{-1}(\boldsymbol{J}_n\boldsymbol{M}^{-1})^{+}\ddot{\tilde{\boldsymbol{r}}}_{nd} \\ & + \boldsymbol{J}_j\boldsymbol{M}^{-1}[\boldsymbol{I}_n - (\boldsymbol{J}_n\boldsymbol{M}^{-1})^{+}(\boldsymbol{J}_n\boldsymbol{M}^{-1})]\,{}^{1}\boldsymbol{l}\end{aligned} \tag{11}$$

Then, noticing the relation of Eq. (6),

$$\begin{aligned}& {}^{1}\ddot{\boldsymbol{r}}_j - \dot{\boldsymbol{J}}_j\dot{\boldsymbol{q}} - \boldsymbol{J}_j\boldsymbol{M}^{-1}(\boldsymbol{J}_n\boldsymbol{M}^{-1})^{+}(\ddot{\boldsymbol{r}}_{nd} - \dot{\boldsymbol{J}}_n\dot{\boldsymbol{q}}) \\ & = \boldsymbol{J}_j\boldsymbol{M}^{-1}[\boldsymbol{I}_n - (\boldsymbol{J}_n\boldsymbol{M}^{-1})^{+}(\boldsymbol{J}_n\boldsymbol{M}^{-1})]\,{}^{1}\boldsymbol{l}\end{aligned} \tag{12}$$

Here, we define three variables shown as

$${}^{1}\ddot{\hat{\boldsymbol{r}}}_j \triangleq \dot{\boldsymbol{J}}_j\dot{\boldsymbol{q}} + \boldsymbol{J}_j\boldsymbol{M}^{-1}(\boldsymbol{J}_n\boldsymbol{M}^{-1})^{+}(\ddot{\boldsymbol{r}}_{nd} - \dot{\boldsymbol{J}}_n\dot{\boldsymbol{q}}) \tag{13}$$

$$\Delta\,{}^{1}\ddot{\boldsymbol{r}}_j \triangleq {}^{1}\ddot{\boldsymbol{r}}_j - {}^{1}\ddot{\hat{\boldsymbol{r}}}_j \tag{14}$$

$${}^{1}\boldsymbol{\Lambda}_j \triangleq \boldsymbol{J}_j\boldsymbol{M}^{-1}[\boldsymbol{I}_n - (\boldsymbol{J}_n\boldsymbol{M}^{-1})^{+}(\boldsymbol{J}_n\boldsymbol{M}^{-1})] \tag{15}$$

In Eq. (13), ${}^{1}\ddot{\hat{\boldsymbol{r}}}_j$ is represents acceleration caused by manipulator's shape change. In the right side of Eq. (13), the first term denotes Coliolis and centrifugal acceleration of j-th link, the second term represents influence of ${}^{1}\ddot{\tilde{\boldsymbol{r}}}_{nd}$ on j-th

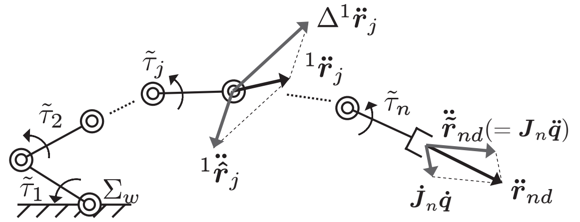

Fig. 3. Reconfiguration at intermediate link during hand task executed

link except Coliolis and centrifugal acceleration at n-th link. Then, Eq. (12) can be rewritten as

$$\Delta^1\ddot{\boldsymbol{r}}_j = {}^1\boldsymbol{\Lambda}_j\,{}^1\boldsymbol{l} \tag{16}$$

The relation between $^1\ddot{\boldsymbol{r}}_j$ and $\Delta^1\ddot{\boldsymbol{r}}_j$ is shown in Fig. 3. However, the problem is whether we can yield desired $\Delta^1\ddot{\boldsymbol{r}}_{jd}$, that is, whether we can find $^1\boldsymbol{l}$ to generate $\Delta^1\ddot{\boldsymbol{r}}_{jd}$. From Eq. (16), we can obtain $^1\boldsymbol{l}$ as

$$^1\boldsymbol{l} = {}^1\boldsymbol{\Lambda}_j^+\Delta^1\ddot{\boldsymbol{r}}_{jd} + (\boldsymbol{I}_n - {}^1\boldsymbol{\Lambda}_j^+\,{}^1\boldsymbol{\Lambda}_j)\,{}^2\boldsymbol{l} \tag{17}$$

In Eq. (17), $^2\boldsymbol{l}$ is an arbitrary vector satisfying $^2\boldsymbol{l} \in \mathrm{R}^n$. Assuming that $^1\boldsymbol{l}$ is restricted as $\|^1\boldsymbol{l}\| \leq 1$, then we obtain next relation,

$$(\Delta^1\ddot{\boldsymbol{r}}_{jd})^T({}^1\boldsymbol{\Lambda}_j^+)^{T\,1}\boldsymbol{\Lambda}_j^+\Delta^1\ddot{\boldsymbol{r}}_{jd} \leq 1 \tag{18}$$

If $rank({}^1\boldsymbol{\Lambda}_j) = m$, Eq. (18) represents an ellipsoid expanding in m-dimensional space, holding

$$\Delta^1\ddot{\boldsymbol{r}}_{jd} = {}^1\boldsymbol{\Lambda}_j{}^1\boldsymbol{\Lambda}_j^+\Delta^1\ddot{\boldsymbol{r}}_{jd}, \qquad \Delta^1\ddot{\boldsymbol{r}}_{jd} \in \mathrm{R}^m, \tag{19}$$

which indicates that $\Delta^1\ddot{\boldsymbol{r}}_{jd}$ can be arbitrarily generated in m-dimensional space and Eq. (16) always has the solution $^1\boldsymbol{l}$ corresponding to all $\Delta^1\ddot{\boldsymbol{r}}_{jd} \in \mathrm{R}^m$. On the other hand, if $rank({}^1\boldsymbol{\Lambda}_j) = r < m$, $\Delta\ddot{\boldsymbol{r}}_{jd}$ does not value arbitrarily in R^m. In this case, reduced $\Delta\ddot{\boldsymbol{r}}_{jd}$ is denoted as $\Delta^1\ddot{\boldsymbol{r}}^*_{jd}$. Then Eq. (18) is written as

$$\begin{aligned}(\Delta^1\ddot{\boldsymbol{r}}^*_{jd})^T({}^1\boldsymbol{\Lambda}_j^+)^T\,{}^1\boldsymbol{\Lambda}_j^+\Delta^1\ddot{\boldsymbol{r}}^*_{jd} \leq 1\\ (\Delta^1\ddot{\boldsymbol{r}}^*_{jd} = {}^1\boldsymbol{\Lambda}_j{}^1\boldsymbol{\Lambda}_j^+\Delta^1\ddot{\boldsymbol{r}}_{jd})\end{aligned} \tag{20}$$

Equation (20) describes an ellipsoid expanded in r-dimensional space. These ellipsoids of Eqs. (18) and (20) are shown in Fig.2(b).

C. Dynamic Reconfiguration Manipulability Shape Index(DRMSI)

In this section, we propose the index evaluating DRM. Thus, by applying the singular value decomposition for this matrix $\boldsymbol{\Lambda}$, we get

$$^1\boldsymbol{\Lambda}_j = {}^1\boldsymbol{U}_j^1\boldsymbol{\Sigma}_j^1\boldsymbol{V}_j^T \tag{21}$$

$$^1\boldsymbol{\Sigma}_j = \begin{array}{c} \\ r \\ \\ m-r \end{array}\overset{\qquad r \qquad\qquad n-r}{\begin{bmatrix} ^1\sigma_{j,1} & & \mathbf{0} & \\ & \ddots & & \mathbf{0} \\ \mathbf{0} & & ^1\sigma_{j,r} & \\ & \mathbf{0} & & \mathbf{0} \end{bmatrix}} \tag{22}$$

In Eqs. (21) and (22), $^1\boldsymbol{U} \in \mathrm{R}^{m\times m}, {}^1\boldsymbol{V} \in \mathrm{R}^{n\times n}$ are orthogonal matrixes, and r denotes the number of non-zero singular values of $^1\boldsymbol{\Lambda}_j$ and $\sigma_{j,1}\geq \cdots \geq\sigma_{j,r} > 0$. In addition, $r\leq m$ because $rank({}^1\boldsymbol{\Lambda}_j)\leq m$. So, dynamic reconfiguration capability of j-th link when hand of manipulator operating task can be described by following equation.

$$^1w_j = {}^1\sigma_{j,1}\cdot{}^1\sigma_{j,2}\cdots{}^1\sigma_{j,r} \tag{23}$$

In this paper, we defined the value of w_j in Eq. (23) as dynamic reconfiguration manipulability measure (DRMM), which indicates the degree of that reconfiguration acceleration of j-th link can be generated for arbitrary direction. And, volume of dynamic reconfiguration ellipsoid at the j-th link is described as $^1V_{DRj}$. Then, in order to consider dynamic reconfiguration measure of the whole manipulator-links, we define a index named dynamic reconfiguration manipulability shape index (DRMSI) as follows:

$$^1W_{DR} = \sum_{j=1}^{n-1} a_j\ {}^1V_{DRj} \tag{24}$$

Here, a_j is unit adjustment between different dimension. In this paper, singular-values increase a hundredfold to enlarge value of ellipsoid, compared to ellipse or line segment.

D. Numerical Examples

In this section, we introduce a numerical example of the proposed DRM for a 4-link manipulator in Fig. 4. Length, mass and coefficient of viscous friction of each link and joint are set to be 0.3[m], 1.0[kg], and 2.0[N·m·s/rad]. In this simulation, we assume that tip of link-2 and link-4 are always placed $y = 0$, that is, when q_2 and q_4 are given, q_1

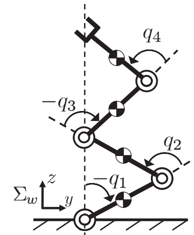

Fig. 4. 4-link manipulator

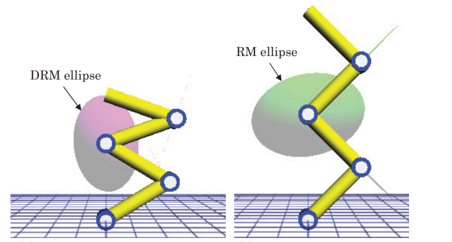

(a) Dynamic reconfiguration manipulability (DRM) ellipse

(b) Reconfiguration manipulability (RM) ellipse

Fig. 5. Shapes of manipulator

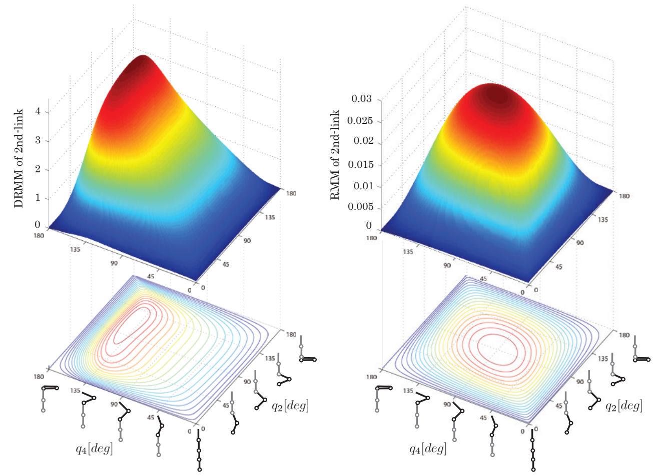

(a) 2nd-link-DRMM distribution

(b) 2nd-link-RMM distribution

Fig. 6. 2nd-link DRMM and RMM distribution

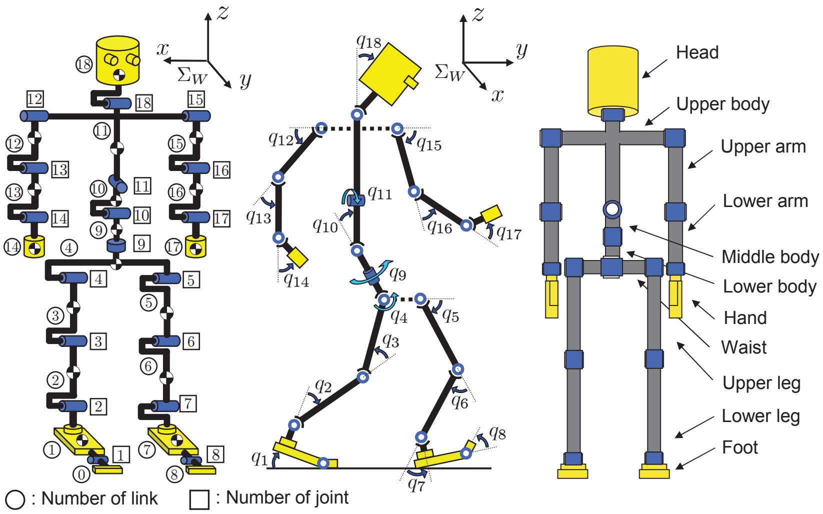

Fig. 7. Definition of humanoid's link, joint and angle number

TABLE I
PHYSICAL PARAMETERS

Link	l_i	m_i	d_i
Head	0.24	4.5	0.5
Upper body	0.41	21.5	10.0
Middle body	0.1	2.0	10.0
Lower body	0.1	2.0	10.0
Upper arm	0.31	2.3	0.03
Lower arm	0.24	1.4	1.0
Hand	0.18	0.4	2.0
Waist	0.27	2.0	10.0
Upper leg	0.38	7.3	10.0
Lower leg	0.40	3.4	10.0
Foot	0.07	1.1	10.0
Total	1.7	63.8	

and q_3 are set as $q_1 = -q_2/2.0$ and $q_3 = -(q_2 + q_4)/2.0$. Figure 5(a) and (b) depict the DRME (scaled) and RME (scaled) with manipulator shapes, which indicate the peak of 2nd-link-DRMM distribution and 2nd-link reconfiguration manipulability measure (RMM) distribution shown in Fig. 6. In Fig. 6, the peak of 2nd-link RMM at $q_2 = 90°$ and $q_4 = 90°$. On the other hand, the peak of 2nd-link DRMM at $q_2 = 118°$ and $q_4 = 141°$.

III. Dynamical Walking Model

We discuss a biped robot whose definition is depicted in Fig. 7. Table I indicates length l_i [m], mass m_i [kg] of links and joints' coefficient of viscous friction d_i [N·m·s/rad], which are decided based on [10]. Our model represents rigid whole body—feet including toe, torso, arms and body—having 18 degree-of-freedom. Detail explanation of this model is omitted, which is described in [11].

IV. Visual Lifting Approach

A. Feedback lifting torque generator

This section presents a vision-feedback control for improving humanoid's standing/walking stability [12] as shown in Fig. 8. Here, the force exerted on the head to minimize $\delta\boldsymbol{\psi}(t) = \boldsymbol{\psi}_d(t) - \boldsymbol{\psi}(t)$ calculated from measured position or pose, we assume this parameter as being detected correctly in this paper. The joint torque $\boldsymbol{\tau}_h(t)$ that pulls the robot's head up is given the following equation:

$$\boldsymbol{\tau}_h(t) = \boldsymbol{J}_h(\boldsymbol{q})^T \boldsymbol{K}_p \delta\boldsymbol{\psi}(t), \tag{25}$$

where $\boldsymbol{J}_h(\boldsymbol{q})$ in Fig. 8 is Jacobian matrix of the head pose against joint angles including $q_1, q_2, q_3, q_4, q_9, q_{10}, q_{11}, q_{18}$, and $\boldsymbol{K}_p$ means proportional gain similar to impedance control. We use this input to compensate the falling motions caused by gravity or dangerous slipping motion happened unpredictably during all walking states in Fig. 9.

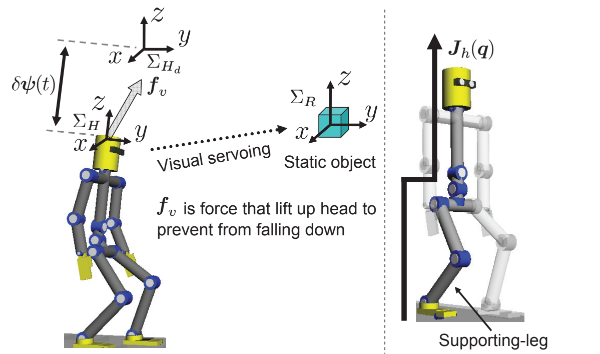

Fig. 8. Concept of Visual Lifting Approach

B. Feedforward leg and body motion generator

In addition to $\boldsymbol{\tau}_h(t)$, we used two input torques: $\boldsymbol{\tau}_t(t) = [0, \cdots, 0, \tau_{t5}, 0, \cdots, 0]^T$ to make floating-leg (joint-5) step forward and $\boldsymbol{\tau}_w(t) = [0, \cdots, 0, \tau_{w11}, 0, \cdots, 0]^T$ to swing waist's roll angle (joint-11) according to supporting-foot. The element τ_{t5} and τ_{w11} of $\boldsymbol{\tau}_t(t)$ and $\boldsymbol{\tau}_w(t)$ are settled by approximate human's walking-cycle as below:

$$\tau_{t5} = 20\cos\{2\pi(t - t_1)/1.85\}, \tag{26}$$

$$\tau_{w11} = \begin{cases} 50\sin\{2\pi(t - t_1)/1.85\} & (if \text{ Right leg}) \\ -50\sin\{2\pi(t - t_1)/1.85\} & (if \text{ Left leg}). \end{cases} \tag{27}$$

Here, t_1 means the time that supporting-foot and contacting-foot are switched, which is gate-transition from (V) and (VII) to (VII).

C. Combined lifting/swinging controller

Combining three torque generators expressed as Eqs. (25), (26) and (27), a controller for walking is created as $\boldsymbol{\tau}(t) = \boldsymbol{\tau}_h(t) + \boldsymbol{\tau}_t(t) + \boldsymbol{\tau}_w(t)$.

V. Example of Bipedal Walking

Under the environment that sampling time was set as 3.0×10^{-3} [sec] and friction force between foot and the ground as $f_t = 0.7 f_{n_z}$, the following simulations were conducted.

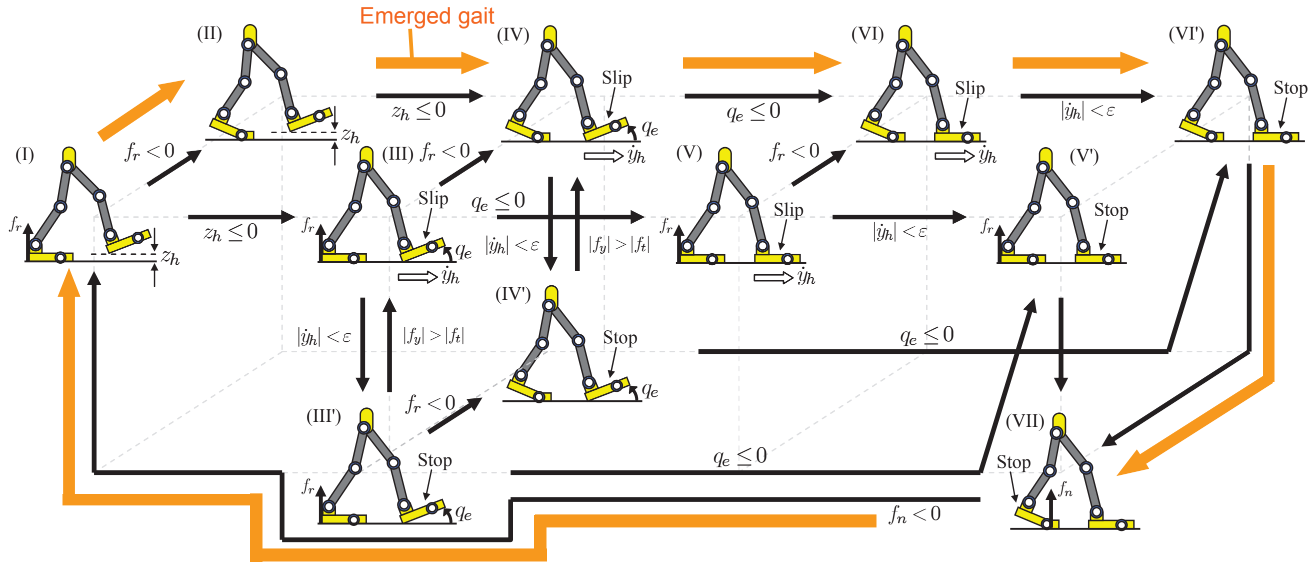

Fig. 9. State, gait's transition and emerged walking gait.

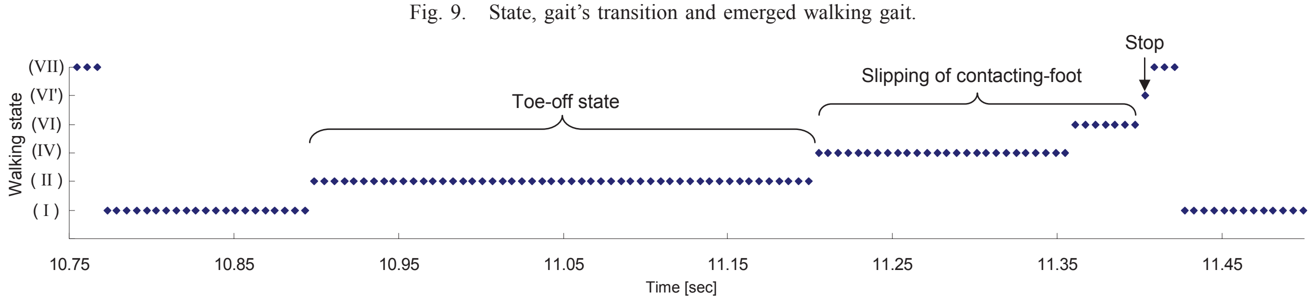

Fig. 10. State transition of walking in one step.

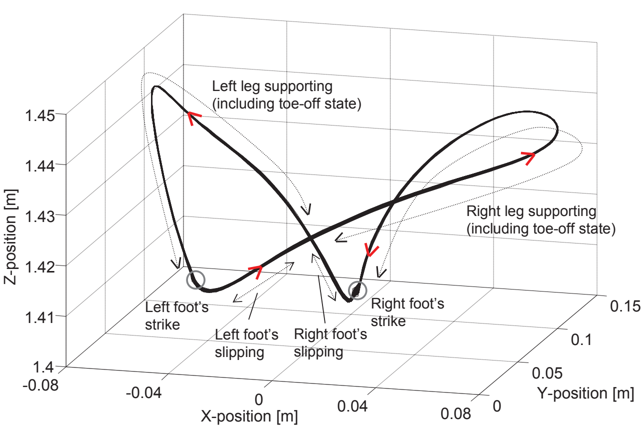

Fig. 11. Emerged limit cycle [(x, y, z) trajectory of neck]

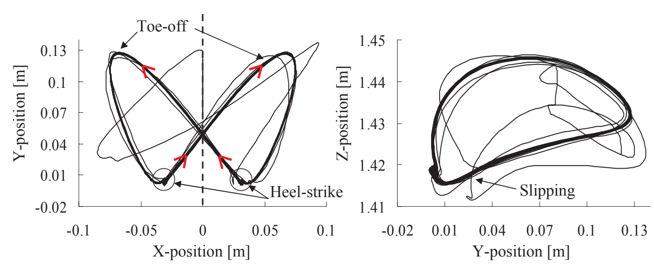

Fig. 12. Motion trajectory of neck

A. Stable Walking by Large Lifting Gain

In this section, we set lifting proportional gain $\boldsymbol{K}_p = diag[20, 290, 1100]$ to achieve stable walking. The humanoid walked as shown Fig. 13(a) and the followings are the results: average length of stride is 0.43 [m] and walking speed is 2.15 [km/h]. Figure 10 show state transition generated by the humanoid's dynamics. In this simulation, the humanoid walked in accordance with the following path: (I) $\rightarrow$ (II) $\rightarrow$ (IV) $\rightarrow$ (VI) $\rightarrow$ (VI$'$) $\rightarrow$ (VII) $\rightarrow$ (I) $\rightarrow \cdots$ in Fig. 9 as "Emerged gait." This transition was selected among all possible transient in Fig. 9 by the closed loop dynamics. Figure 11 depicts trajectory of neck (origin of link-18) in 3-D space representation, excluding a trajectory in transient state corresponding to 0–20 steps, this means that the walking motion converged into limit cycle after 21 walking steps. Then, the trajectories that are separated into two plane (x-y plane and y-z plane) from initial condition to 200 steps are shown in Fig. 12. We can confirm that motion concerning left side and right side against the dotted line is symmetric, which means the neck and shoulder swung along with y-axis given at Fig. 12, representing rolling motion of upper body. The right graph representing neck's motion in y-z plane, the neck swayed in sagittal plane forward and backward with height varying by walking states including heel-striking (contacting) state in it. These figures implies that visual feedback has stabilized the walking including gait's transition and motions as shown in Fig. 9, including toe-off state, heel-striking, slipping and change of state variables.

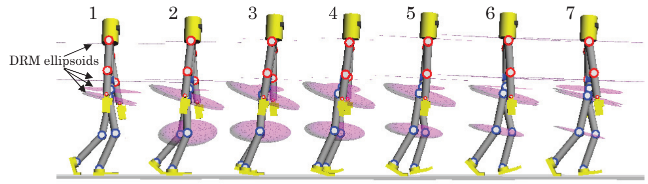

(a) Large lifting-gain $(\boldsymbol{K}_p = diag[20, 290, 1100])$

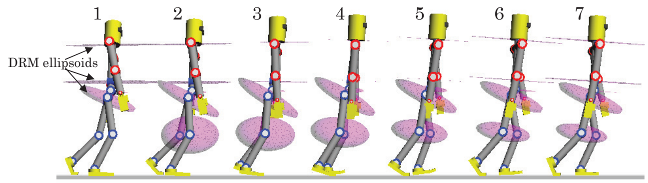

(b) Medium lifting-gain $(\boldsymbol{K}_p = diag[20, 290, 950])$

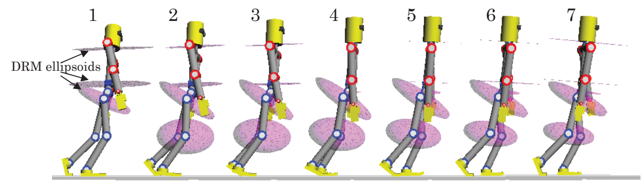

(c) Small lifting-gain $(\boldsymbol{K}_p = diag[20, 290, 900])$

Fig. 13. Screen-shot of bipedal walking with DRM ellipsoids

B. Analyses based on Dynamic Reconfiguration Manipulability

In this section, three kinds of lifting-proportional-gain are set to be $\boldsymbol{K}_p = diag[20, 290, 1100]$ (Large lifting-gain), $\boldsymbol{K}_p = diag[20, 290, 950]$ (Medium lifting-gain) and $\boldsymbol{K}_p = diag[20, 290, 900]$ (Small lifting-gain) to compare walkings by DRM. The humanoid walked as shown Fig. 13(a), (b) and (c), respectively (scaling ellipsoids). Then, there are no DRM ellipsoids (existing line segments) at knee of (a)-1, (b)-1 and (c)-1, since supporting-foot is surface-contacting, that is, joint angles $\boldsymbol{q} = [q_2, q_3, \cdots, q_{18}]^T$. On the other hand, there are DRM ellipsoids (ellipses) at knee of the other phases, since supporting-foot is point-contacting, that is, joint angles $\boldsymbol{q} = [q_1, q_2, \cdots, q_{18}]^T$. In Fig. 13, shapes of (c) crouches down, compared to (a). Furthermore, DRM ellipsoids volume of (c) is larger than (a). In Figs. 14 and 15, as lifting gain larger, DRMSI representing whole volume of DRM ellipsoids is smaller. This means walking of (c) has higher shape-changeability than (a), but it seems that walking of (c) is far from human's walking.

VI. Conclusion

In this paper, we propose a new index for dynamic ability to change configuration as a subsegment redundancy utilization, named Dynamic Reconfiguration Manipulability (DRM), and demonstrate the manipulability with numerical examples for a 4-link manipulator and a humanoid robot. In addition, we introduced Lifting Approach which grantees to keep the posture of humanoid robot stable. And, we confirmed that the robot with walking shape of crouching down has higher dynamic ability to change configuration than walking shape of stretching humanoid's leg.

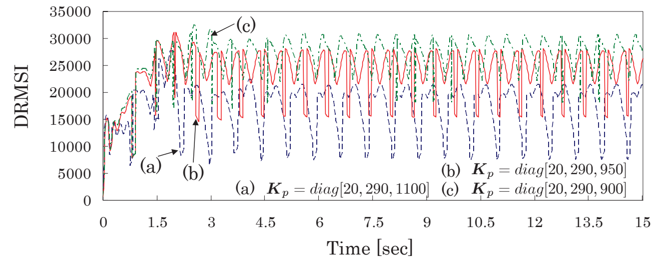

Fig. 14. DRMSI until $t = 15.0[s]$

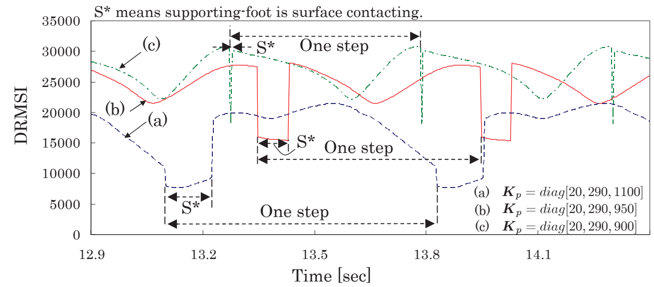

Fig. 15. DRMSI around $t = 13.5[s]$

References

[1] M. Vukobratovic, A. Frank and D. Juricic, "On the Stability of Biped Locomotion," *IEEE Transactions on Biomedical Engineering*, Vol. 17, No. 1, 1970.

[2] M. Vukobratovic and J. Stepanenko, "On the Stability of Anthropomorphic Systems," *Mathematical Biosciences*, Vol. 15, pp. 1–37, 1972.

[3] S. Colins, A. Ruina, R. Tedrake and M. Wisse, "Efficient Bipedal Robots Based on Passive-Dynamic Walkers," *Science*, Vol. 307, pp. 1082–1085, 2005.

[4] J. Pratt, P. Dilworth and G. Pratt, "Virtual Model Control of a Bipedal Walking Robot," *Proceedings of IEEE International Conference on Robotics and Automation*", pp. 193–198, 1997.

[5] R.E. Westervelt, W.J. Grizzle and E.D. Koditschek, "Hybrid Zero Dynamics of Planar Biped Walkers," *IEEE Transactions on Automatic Control*, Vol. 48, No. 1, pp. 42–56, 2003.

[6] Y. Harada, J. Takahashi, D. Nenchev and D. Sato, "Limit Cycle Based Walk of a Powered 7DOF 3D Biped with Flat Feet," *Proceedings of IEEE/RSJ International Conference on Intelligent Robots and Systems*, pp. 3623–3628, 2010.

[7] Y. Huang, B. Chen, Q. Wang, K. Wei and L. Wang, "Energetic efficiency and stability of dynamic bipedal walking gaits with different step lengths," *Proceedings of IEEE/RSJ International Conference on Intelligent Robots and Systems*, pp. 4077–4082, 2010.

[8] T. Wu, T. Yeh and B. Hsu, "Trajectory Planning of a One-Legged Robot Performing Stable Hop," *Proceedings of IEEE/RSJ International Conference on Intelligent Robots and Systems*, pp. 4922–4927, 2010.

[9] Y. Nakamura and K. Yamane, "Dynamics of Kinematic Chains with Discontinuous Changes of Constraints—Application to Human Figures that Move in Contact with the Environments—," *Journal of RSJ*, Vol. 18, No. 3, pp. 435–443, 2000 (in Japanese).

[10] M. Kouchi, M. Mochimaru, H. Iwasawa and S. Mitani, "Anthropometric database for Japanese Population 1997-98," Japanese Industrial Standards Center (AIST, MITI), 2000.

[11] T. Maeba, M. Minami, A. Yanou, J. Nishiguchi, "Dynamical Analyses of Humanoid's Walking by Visual Lifting Stabilization Based in Event-driven State Transition Cooperative manipulations based on Genetic Algorithms using contact information," *2012 IEEE/ASME Int. Conf. on Advanced Intelligent Mechatronics Proc.*, pp. 7–14, 2012.

[12] W. Song, M. Minami, F. Yu, Y. Zhang, "A Visual Lifting Approach for Dynamic Bipedal Walking," *International Journal of Advanced Robotic Systems*, Vol. 9, ISBN: 1729–8806, 2012.

[13] F. Yu, W. Song and M. Minami, "Visual Servoing with Quick Eye-Vergence to Enhance Trackability and Stability," *Proceedings of IEEE/RSJ International Conference on Intelligent Robots and Systems*, pp. 6228–6233, 2010.

[14] T. Yoshikawa, "Dynamic Manipulability of Robot Manipulators," *Proceedings of the IEEE International Conference on Robotics and Automation*, Vol. 2, No. 1, pp. 113–124, 1985.

[15] M. Minami, Y. Naitoh and T. Asakura, "Avoidance Manipulability for Redundant Manipulators," *Journal of the Robotics Society of Japan*, Vol. 17, No. 6, pp. 887–895, 1999 (in Japanese).